International Journal of
Molecular Sciences

MDPI

Article

Euphraticanoids N–T: Aromadendrane-Type Diterpenes and Sesquiterpenes with Fungicidal Activities from *Populus euphratica* Resins

Qinbin Jiang [1,2,†], Yun-Yun Liu [2,†], Danling Huang [2] and Yong-Xian Cheng [1,2,*]

[1] School of Pharmacy, Guangdong Pharmaceutical University, Guangzhou 510006, China; jqb0925@163.com
[2] Guangdong Provincial Key Laboratory of Chinese Medicine Ingredients and Gut Microbiomics, Institute for Inheritance-Based Innovation of Chinese Medicine, School of Pharmacy, Shenzhen University, Shenzhen 518055, China; liuyy@szu.edu.cn (Y.-Y.L.); leonchemistry@szu.edu.cn (D.H.)
* Correspondence: yxcheng@szu.edu.cn; Tel.: +86-0755-2690-2073
† These authors contributed equally to this work.

Abstract: Seven previously undescribed terpenoids, including five prenylaromadendrane-type diterpenes euphraticanoids N–R (**1**–**5**) and two aromadendrane-type sesquiterpenes, euphraticanoids S and T (**6** and **7**), were isolated from *Populus euphratica* resins. Their structures, including their absolute configurations, were elucidated by HRESIMS and spectroscopic analysis, ECD calculations, and crystallographic methods. In addition, an evaluation of the fungicidal activities of compound **1** was carried out, resulting in the discovery of **1** as a fungicidal candidate lead compound with an EC_{50} of 15.7 and 68.6 mg/L against *Curvularia mebaldsii* and *Fusarium graminearum*, respectively.

Keywords: *Populus euphratica* resins; prenylaromadendrane-type diterpenes; aromadendrane-type sesquiterpenes; fungicidal activity

Academic Editor: Cheng-Yang Huang

Received: 16 February 2025
Revised: 25 February 2025
Accepted: 26 February 2025
Published: 28 February 2025

Citation: Jiang, Q.; Liu, Y.-Y.; Huang, D.; Cheng, Y.-X. Euphraticanoids N–T: Aromadendrane-Type Diterpenes and Sesquiterpenes with Fungicidal Activities from *Populus euphratica* Resins. *Int. J. Mol. Sci.* **2025**, *26*, 2187. https://doi.org/10.3390/ijms26052187

1. Introduction

All living creatures, including humans, animals, and plants, have developed diverse defense strategies though evolution for self-protection, as they face extreme stresses such as environmental stresses and social stresses. Among various defense mechanisms, exudate production plays an important role. For example, humans shed tears when they get hurt; the hagfish produces slime when it is provoked [1]; sperm whales create ambergris when they eat hard squid beak chitin, an irritant [2]; and *Megaponera analisantis* ants secrete saliva to treat infected wounds when nestmates are infected [3]. However, the phenomenon of resinous exudate production to defend against injury is more common in plants than humans and animals, such as agarwood from the resinous heartwood of *Aquilaria* tree [4]; red resin from the fruits of *Daemonorops draco* tree [5]; yellowish resins from *Ferula sinkiangensis* [6], and so on. We assumed that these plants' resinous exudates are used to defend, and should have biological activities, which also suggested that these resins may be a potentially valuable reservoir in drug discovery. Therefore, our group has focused on plant resins in recent years. A recent comprehensive review by us summarized the chemistry and biological activity of recent substances, highlighting our contribution to this field [7]. The tears of *Populus euphratica* were collected for systematic research by us, accompanied by discovering a series of structurally intriguing and biologically significant compounds, including various terpenoids [8]. As a continuous study on this topic, five prenylaromadendrane-type diterpenes euphraticanoids N–R (**1**–**5**) and two

aromadendrane-type sesquiterpenes euphraticanoids S and T (**6** and **7**) were identified (Figure 1). In addition, we evaluated the fungicidal activity of compounds **1**–**7**. As a result, compound **1** was found to exhibit potent fungicidal activity against *Curvularia mebaldsii* and *Fusarium graminearum*. This finding provides hope for the discovery of fungicides derived from *P. euphratica.*

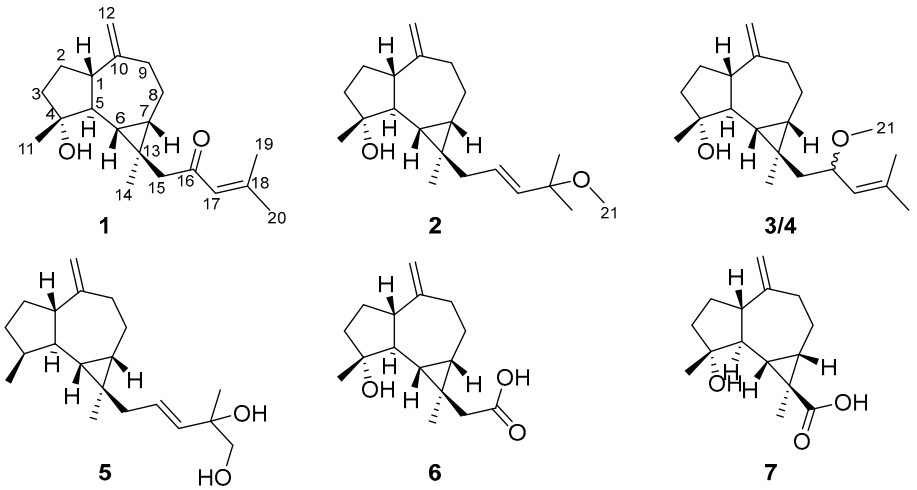

Figure 1. The chemical structures of compounds **1**–**7**.

2. Results and Discussion

2.1. Compound Structure Elucidation

Euphraticanoid N (**1**) was obtained as yellowish crystals through crystallization of methanol, and its molecular formula $C_{20}H_{30}O_2$ was supported by HRESIMS (*m*/*z* 303.2311 $[M + H]^+$, calcd for $C_{20}H_{31}O_2$, 303.2319), ^{13}C NMR, and DEPT spectra. The ^1H NMR spectrum (Table 1) showed signals for four methyl groups at δ_H 2.14 (3H, d, *J* = 0.8 Hz), 1.87 (3H, d, *J* = 0.8 Hz), 1.24 (3H, s), and 1.03 (3H, s), and three olefinic protons at δ_H 6.00 (1H, brs), 4.73 (1H, brs), and 4.69 (1H, brs), along with two characteristic protons at δ_H 0.60 (1H, t-like, *J* = 11.0 Hz) and 0.77 (1H, td, *J* = 11.0, 6.6 Hz). According to the ^{13}C NMR and DEPT spectra (Table 2), there were twenty distinct carbon resonances, categorized into four methyl groups, six methylene groups, five methine groups, and five signals from nonprotonated carbons (one ketocarbonyl group at δ_C 201.0, two olefinic groups at δ_C 155.8 and 154.3, one oxygenated group at δ_C 79.8, and one sp^3 quaternary carbon). The data mentioned above indicated that compound **1** is a prenylaromadendrane-type diterpene, and 1D NMR data analysis suggested that the signals of **1** were similar to those of 4β-hydroxy-15-(3-methyl-2-butenyl) aromadendr-$\Delta^{10(12)}$-en [9]. In the ^{13}C NMR spectrum, a key difference was that the methylene singlet at δ_C 25.6 (C-16) was substituted by a ketone carbonyl signal at δ_C 201.0, along with a downfield shift in C-15 (δ_C 39.1→δ_C 56.6) and C-18 (δ_C 131.2→δ_C 155.8) carbon signals adjacent to C-16. Furthermore, the specific UV absorption wavelength (239 nm) combined with the molecular weight of **1** suggested that the methylene at C-16 was transformed into a ketone carbonyl, forming an α,β-unsaturated ketone carbonyl group with the double bond between C-17 and C-18. The conclusion also was further supported by the HMBC correlations (Figure 2) of H_2-15/C-16 (δ_C 201.1), C-17 (δ_C 124.1), and H_3-19/C-17, C-18 (δ_C 155.8). As a result, the planar structure of **1** was determined (Figure 1).

Table 1. ^{1}H NMR (600 MHz) data for **1–4** (δ in ppm, J in Hz).

No	1 [a]	2 [b]	3 [b]	4 [b]
1	2.28, m	2.27, overlap	2.26, overlap	2.26, overlap
2	Ha: 1.94, m Hb: 1.68, overlap	Ha: 2.27, overlap Hb: 1.68, m	Ha: 2.26, overlap Hb: 1.68, m	Ha: 2.26, overlap Hb: 1.67, overlap
3	Ha: 1.84, m Hb: 1.68, overlap	Ha: 2.05, m Hb: 1.67, m	Ha: 2.04, m Hb: 1.67, m	Ha: 2.05, m Hb: 1.67, overlap
5	1.43, t (11.0)	1.74, t (10.5)	1.72, t (10.4)	1.77, t (10.3)
6	0.60, t-like (11.0)	0.64, t-like (10.5)	0.61, t (10.4)	0.58, t (10.4)
7	0.77, td (11.0, 6.6)	0.77, td (10.5, 6.1)	0.79, td (10.4, 6.4)	0.94, td (10.4, 6.4)
8	Ha: 2.02, m Hb: 0.99, m	Ha: 1.97, m Hb: 1.13, m	Ha: 1.93, dt (13.0, 6.4) Hb: 1.08, q-like (13.0)	Ha: 2.03, m Hb: 1.15, q-like (12.8)
9	Ha: 2.43, dd (13.0, 6.5) Hb: 1.98, m	Ha: 2.48, dd (13.2, 5.9) Hb: 2.14, t (13.2)	Ha: 2.48, dd (13.0, 6.4) Hb: 2.12, t (13.0)	Ha: 2.48, dd (12.8, 6.0) Hb: 2.13, t (12.8)
11	1.24, s	1.54, s	1.51, s	1.54, s
12	Ha: 4.73, br s Hb: 4.69, br s	Ha: 4.89, br s Hb: 4.80, br s	Ha: 4.88, br s Hb: 4.81, br s	Ha: 4.89, br s Hb: 4.81, br s
14	1.03, s	1.17, s	1.21, s	1.28, s
15	Ha: 2.83, d (17.9) Hb: 1.95, d (17.9)	Ha: 2.06, m Hb: 2.03, m	Ha: 2.02, dd (13.7, 6.6) Hb: 1.27, dd (13.7, 6.6)	Ha: 1.63, dd (14.3, 4.1) Hb: 1.57, dd (14.3, 8.4)
16		5.77, td (15.7, 7.1)	4.21, dt (9.4, 6.6)	4.23, td (8.4, 4.1)
17	6.00, br s	5.66, d (15.7)	5.14, d (9.4)	5.20, br d (8.4)
19	1.87, d (0.8)	1.31, s	1.75, s	1.72, br s
20	2.14, d (0.8)	1.31, s	1.70, s	1.70, br s
21		3.19, s	3.27, s	3.28, s
4-OH		5.37, s	5.15, s	5.29, s

[a] NMR spectra data were recorded in $CDCl_3$. [b] NMR spectra data were recorded in pyridine-d_5.

Table 2. ^{13}C NMR (150 MHz) data for **1–7** (δ in ppm).

No	1 [a]	2 [b]	3 [b]	4 [b]	5 [b]	6 [a]	7 [a]
1	49.0, CH	54.3, CH	53.4, CH	54.0, CH	54.0, CH	49.1, CH	52.2, CH
2	24.2, CH_2	27.6, CH_2	27.2, CH_2	27.5, CH_2	29.8, CH_2	24.3, CH_2	26.8, CH_2
3	39.5, CH_2	43.0, CH_2	42.5, CH_2	42.9, CH_2	35.6, CH_2	39.5, CH_2	41.2, CH_2
4	79.8, C	80.3, C	80.2, C	80.2, C	36.2, CH	80.5, C	81.2, C
5	53.5, CH	54.3, CH	54.3, CH	54.3, CH	44.1, CH	53.3, CH	52.9, CH
6	24.7, CH	29.9, CH	29.9, CH	30.0, CH	28.3, CH	24.9, CH	32.4, CH
7	26.5, CH	26.8, CH	27.3, CH	27.8, CH	26.6, CH	26.9, CH	31.2, CH
8	25.1, CH_2	25.5, CH_2	25.6, CH_2	25.5, CH_2	25.4, CH_2	25.2, CH_2	24.6, CH_2
9	39.1, CH_2	39.6, CH_2	39.7, CH_2	39.7, CH_2	39.6, CH_2	38.9, CH_2	38.4, CH_2
10	154.3, C	154.4, C	154.7, C	154.6, C	154.7, C	154.0, C	152.3, C
11	23.9, CH_3	27.3, CH_3	26.6, CH_3	26.9, CH_3	18.0, CH_3	23.9, CH_3	25.9, CH_3
12	106.7, CH_2	106.7, CH_2	106.7, CH_2	106.6, CH_2	106.4, CH_2	107.0, CH_2	107.7, CH_2
13	20.5, C	24.9, C	22.7, C	23.2, C	24.7, C	21.0, C	30.3, C
14	14.5, CH_3	14.6, CH_3	14.9, CH_3	15.3, CH_3	14.0, CH_3	14.3, CH_3	23.5, CH_3
15	56.6, CH_2	46.4, CH_2	49.6, CH_2	49.8, CH_2	46.3, CH_2	46.2, CH_2	177.4, C
16	201.0, C	128.6, CH	76.6, CH	76.9, CH	126.7, CH	176.6, C	
17	124.1, CH	137.8, CH	127.9, CH	128.2, CH	138.7, CH		
18	155.8, C	75.2, C	135.3, C	134.9, C	73.6, C		
19	27.9, CH_3	26.9, CH_3	26.2, CH_3	26.2, CH_3	25.9, CH_3		
20	21.0, CH_3	26.2, CH_3	18.6, CH_3	18.6, CH_3	71.5, CH_3		
21		50.5, CH_3	55.6, CH_3	55.8, CH_3			

[a] NMR spectra data were recorded in $CDCl_3$. [b] NMR spectra data were recorded in pyridine-d_5.

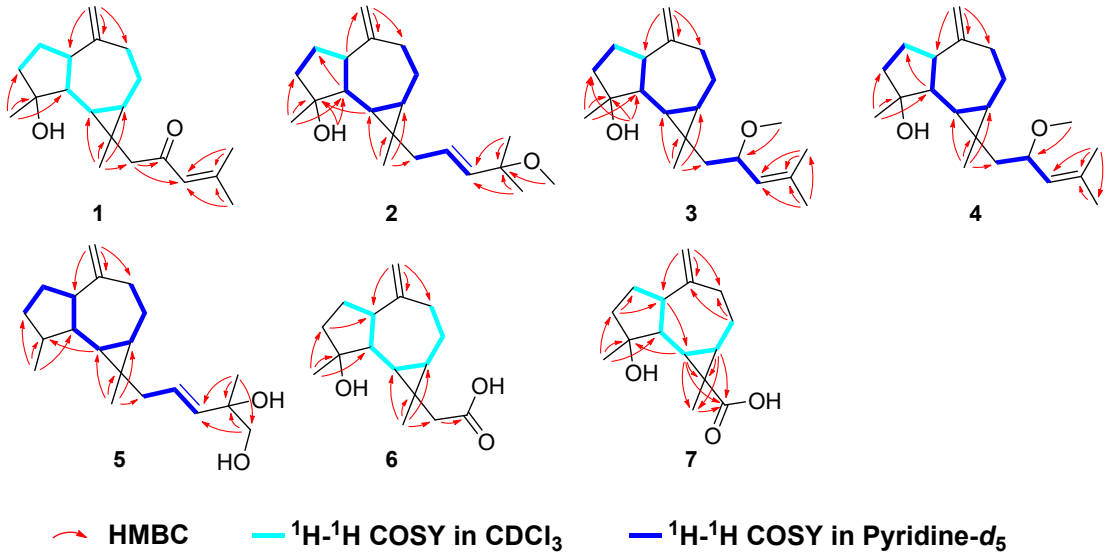

Figure 2. ^{1}H-^{1}H COSY and key HMBC correlations of **1**–**7**.

To establish the relative configuration of **1,** a ROESY experiment was conducted. The ROESY correlations (Figure 3) between H-7/Ha-15, H-1 (weak), H-6/Ha-15, H-1, H_3-11, and H_3-14/H-5 implied that H-6, H-7, H-1, CH_3-11, and H_2-15 were on the same face and β-oriented, while CH_3-14 and H-5 were α-oriented. The absolute configuration of compound **1** was identified through electronic circular dichroism (ECD) calculations at the B3LYP/6-311g(d,p) level. The data demonstrated that the ECD spectrum calculated for (1*S*,4*R*,5*S*,6*S*,7*S*,13*R*)-**1** (Figure 4) were very similar to the experimental spectrum, confirming the absolute configuration of **1** as 1*S*,4*R*,5*S*,6*S*,7*S*,13*R*. Luckily, a suitable crystal of **1** was acquired, and X-ray diffraction analysis with CuKα radiation was performed (Figure 4), confirming the previous conclusion.

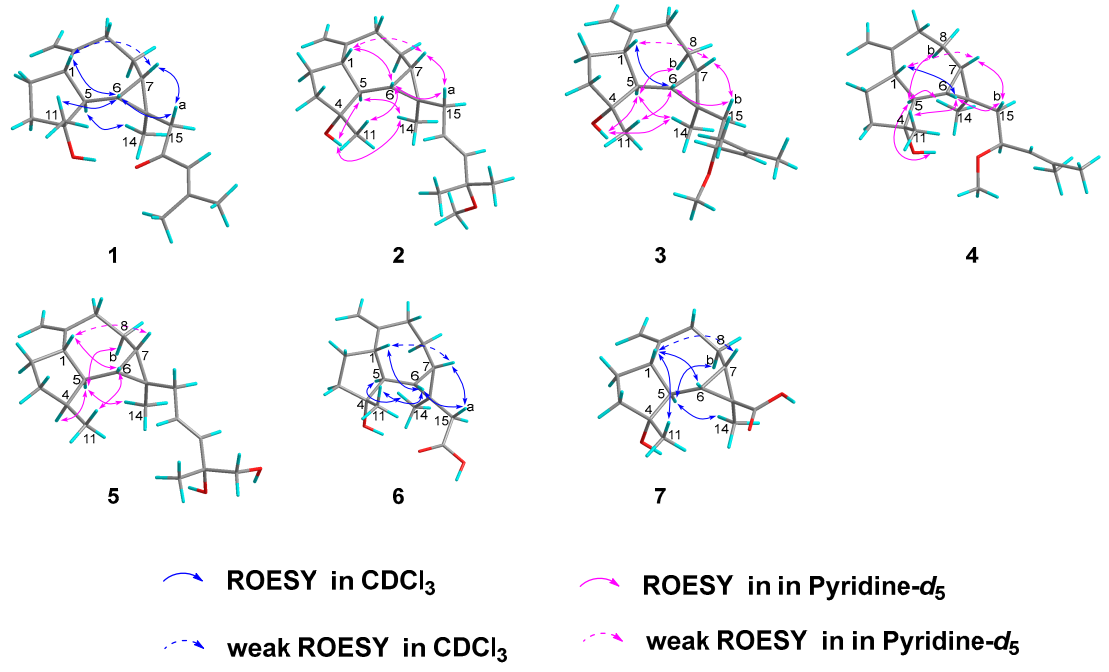

Figure 3. Key ROESY correlations of **1**–**7**.

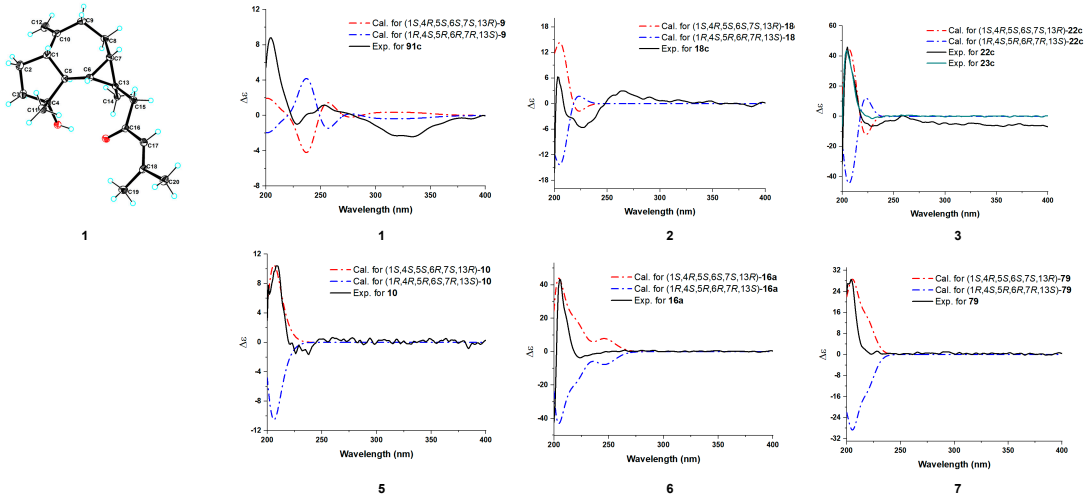

Figure 4. X-ray structures of **1**. Comparison of B3LYP/6-311g(d,p) calculated ECD spectra together with the experimental spectra of **1**–**7** in MeOH. **1**: σ = 0.3 eV; shift = 11 nm, scaling factor = 2.5; **2**: σ = 0.29 eV, shift = 10 nm, scaling factor = 0.9; **3/4**: σ = 0.29 eV; shift = 25 nm, scaling factor = 1.53; **5**: σ = 0.29 eV, shift = 10 nm, scaling factor = 1.67; **6**: σ = 0.35 eV, shift = 23 nm, scaling factor = 4.5; **7**: σ = 0.27 eV, shift = 0 nm, scaling factor = 26.5.

Euphraticanoid O (**2**) was isolated as a colorless gum, with a molecular formula of $C_{21}H_{34}O_2$, determined from the HRESIMS ion peak at m/z 341.2452 $[M + H]^+$ (calcd for $C_{21}H_{35}O_2$, 341.2451). According to the ^1H and ^{13}C NMR data (Tables 1 and 2), compound **2** resembled boscartol C [10], except for a methoxyl group resonating at δ_H/δ_C 3.19/50.5 (CH_3-21) in pyridine-d_5 instead of the hydroxy group. This was corroborated by the HMBC correlations (Figure 2) of H_3-21/C-18 (δ_C 75.2), H_3-18/C-17, C-18, and H_3-19/C-17, C-18. Additionally, compound **2** shared the same relative configurations at the chiral centers in C-1, C-4, C-5, C-6, C-7, and C-13 as **1**, based on similar findings in the 1D NMR (Tables 1 and 2) and ROESY spectra (Figure 3). Moreover, the large coupling constant of H-17 (J = 15.7 Hz) indicated that the double bond between H-16 and H-17 is an *E* configuration. Finally, the absolute configuration of **2** as 1*S*,4*R*,5*S*,6*S*,7*S*,13*R* was validated through the comparison of the experimental and calculated ECD curves (Figure 4).

Euphraticanoid P (**3**) was identified with a molecular formula of $C_{21}H_{34}O_2$, derived from the positive HRESIMS data. In the ^1H and ^{13}C NMR data (Tables 1 and 2) for compound **3**, there were strong resemblances to compound **1**, with the exception of the missing ketone resonance at δ_C 201.0 (C-16). Instead, oxymethine signals were detected at δ_H/δ_C 4.14/75.7 (CH-16) in $CDCl_3$ in the 1D NMR spectra of **3**. Furthermore, more shielded resonances of protons for Ha-15 (δ_H 2.83→δ_H 1.52), Hb-15 (δ_H 1.95→δ_H 1.25), and H-17 (δ_H 6.00→δ_H 4.95), and carbons for C-15 (δ_C 56.6→δ_C 48.8) and C-18 (δ_C 155.8→δ_C 135.7) in $CDCl_3$ were observed due to the conversion from a ketone carbonyl to an methoxyl group at C-16, as confirmed by the ^1H-^1H COSY correlations (Figure 2) of H_2-15/H-16/H-17 and the HMBC correlations (Figure 2) of H_3-21/C-16. Then, based on ROESY correlations and 1D NMR data similar to those of **1** and **2**, the relative configuration of 1*S**,4*R**,5*S**,6*S**,7*S**,13*R** in **3** was identified. The relative configuration of C-16 was not assigned because the flexible side chain at C-16 poses a significant challenge. Ultimately, the absolute configuration of compound **3** was identified as 1*S*,4*R*,5*S*,6*S*,7*S*,13*R* by comparing the experimental CD curve with the calculated ECD curve (Figure 4).

Euphraticanoid Q (**4**) was isolated as a colorless gum and had the same molecular formula as **3**, as determined by HRESIMS analysis. Detailed analysis of the 1D NMR spectra revealed that the ^{13}C NMR data for **4** match those of **3**. However, the ^{1}H NMR data showed slight differences, such as (A) variations in the chemical shift, primarily at H-6 (δ_H 0.79→δ_C 0.94), Ha-15 (δ_H 2.02→δ_C 1.63), Hb-15 (δ_H 1.27→δ_C 1.57), and H-17 (δ_H 5.14→δ_C 5.20), and (B) changes in the splitting pattern of oxymethine proton at δ_H 4.21 from *dt* (*J* = 9.4, 6.6) to *td* (*J* = 8.4, 6.6 Hz), indicating that **4** was the C-16-epimer of **3**. Furthermore, the conclusion was reinforced by identical ROESY correlations (Figure 3) involving H-6/H-1, Hb-15, H_3-11, H-7/H-1 (weak), Hb-15, and H-5/Hb-8, H_3-14, 4-OH, and the experimental ECD spectrum in **4** the same as **3**.

Euphraticanoid R (**5**) was isolated as a colorless gum with a molecular formula of $C_{20}H_{32}O_2$, as revealed by HRESIMS. The primary characteristics of the 1D NMR spectra (Tables 2 and 3) for compound **5** was similar to those for compound **2**, except that the hydroxy group signal at C-4 was absent and a hydroxymethyl group (δ_H 3.98, d, *J* = 10.4 Hz and 3.93, d, *J* = 10.4 Hz; δ_C 71.5) appeared at C-20 in the place of a methyl group. These modifications were verified by the change in splitting pattern of the methyl group at C-4 from *s* to *d* (*J* = 8.6 Hz) and the HMBC correlations (Figure 2) involving H_3-11/C-3, C-4, C-5 and H_2-20/C-17 (δ_C 138.7), C-18 (δ_C 73.6). The ROESY correlations of H-6/H-1, H_3-11, H-1/H-7 (weak) and H-5/H-4, H_3-14, Hb-8 were used to define its relative configuration as 1*S**,4*S**,5*S**,6*R**,7*S**,13*R**. In conclusion, the resemblance of the ECD curves of **5** to those of **1**–**4** (Figure 4) implied that the absolute configuration of **5** is 1*S*,4*S*,5*S*,6*R*,7*S*,13*R*.

Table 3. ^{1}H NMR (600 MHz) data of **5**–**7** (δ in ppm, J in Hz).

No	5 [b]	6 [a]	7 [a]
1	2.17, m	2.30, m	2.18, td (10.7, 6.6)
2	Ha: 1.66, m	Ha: 1.95, m	Ha: 1.92, m
	Hb: 1.57, m	Hb: 1.67, m	Hb: 1.67, m
3	Ha: 1.79, ddd (12.6, 6.4, 3.2)	Ha: 1.81, m	Ha: 1.86, m
	Hb: 1.16, m	Hb: 1.68, m	Hb: 1.57, ddd (12.7, 10.4, 6.5)
4	2.03, m		
5	1.39, q (10.4)	1.41, t (10.8),	1.95, t (10.7)
6	0.65, t (10.4)	0.73, t (10.8)	0.98, t-like (10.7)
7	0.74, td (10.4, 6.6)	0.88, td (10.8, 6.8)	1.20, td (10.7, 6.1)
8	Ha: 1.90, dt (12.5, 6.1)	Ha: 2.05, dt (14.6, 6.8)	Ha: 2.03, m
	Hb: 1.04, m	Hb: 0.98, m	Hb: 1.45, q-like (12.3)
9	Ha: 2.42, dd (13.1, 6.1)	Ha: 2.43, dd (13.2, 6.8)	Ha: 2.44, dd (13.6, 6.4)
	Hb: 2.05, m	Hb: 1.99, m	Hb: 2.01, m
11	1.01, d (8.6)	1.29, s	1.35, s
12	4.76, s	Ha: 4.74, br s	Ha: 4.72, br s
		Hb: 4.71, br s	Hb: 4.69, br s
14	1.00, s	1.08, s	1.35, s
15	2.06, m	Ha: 2.68, d (16.8)	
		Hb: 1.87, d (16.8)	
16	6.18, dt (15.0, 7.1)		
17	6.03, d (15.0)		
19	1.67, (s)		
20	3.98, d (10.4)		
	3.93, d (10.4)		

[a] NMR spectra data were recorded in $CDCl_3$. [b] NMR spectra data were recorded in pyridine-d_5.

Euphraticanoid S (**6**) was confirmed to be $C_{16}H_{24}O_3$ using its HRESIMS and ^{13}C NMR data. The 1D and 2D NMR data (Tables 2 and 3) exhibited structural characteristics identical to those of spathulenol [9]. The primary distinction was the presence of an acetate moiety (δ_H/δ_C 2.68, 1.87/46.2; δ_C 176.6) at C-13, instead of a methyl group in **6**, as indicated by the HMBC correlations (Figure 2) of H_3-14/C-6, C-7, C-13, C-15, and H_2-15/C-16 (δ_C 176.6). The ROESY correlations (Figure 3) involving H-6/H-1, Ha-15, H_3-11, H-7/H-1 (weak), Ha-15, and H-5/H_3-14 indicated that H-1, H-6, H-7, H_3-11, and H_2-15 were β-oriented, while H-5 and H_3-14 were α-oriented. Finally, the absolute configuration of **6** was identified as 1*S*,4*R*,5*S*,6*S*,7*S*,13*R* by comparing the calculated ECD spectra with the experimental results (Figure 4).

Euphraticanoid T (**7**) was isolated as white solids, with a molecular formula of $C_{15}H_{22}O_3$ determined through HRESIMS data. The signals in the ^1H and ^{13}C NMR spectra (Tables 2 and 3) were almost identical to those of **6**, except for the substitution of the acetate moiety at C-13 with a carboxyl group, confirmed by the HMBC correlations (Figure 2) of H-7/C-13, C-14, C-15 (δ_C 177.4), H-6/C-13, C-14, C-15, and H_3-14/C-15. Moreover, the ROESY correlations (Figure 3) of H-1/H_3-14, H-6, H-7 (weak), and H-5/H_3-14 were used to determine the β-orientation of the carboxyl group. The absolute configuration was determined to be 1*S*,4*R*,5*S*,6*S*,7*S*,13*R* by comparing the calculated and experimental ECD spectra.

2.2. Biological Activity

The fungicidal activities of compounds against *Fusarium graminearum*, *Curvularia mebaldsii*, *Curvularia lunata*, *Botrytis cinerea*, *Alternaria altanata*, *Sclerotinia sclerotiorum*, and *Rhizoctonia solani* were evaluated, with the commercial fungicide hymexazol used as a positive control. For all compounds, preliminary screening was carried out at a concentration of 80 mg/L, and the results are shown in Table 4. It revealed that these compounds display board-spectrum fungicidal activities. In particular, compounds **1**–**5** show considerable fungicidal activities, which possess inhibitory rates (IRs) of over 50% towards most pathogenic fungi. Among them, compound **1** displays notable anti-*C. mebaldsii* with 80% IRs, whose activity far surpasses that of hymexazol. Given the sufficient quantity and attractive fungicidal activities against *F. graminearum* and *C. mebaldsii* of compounds **1** and **2** in preliminary screening, their maximal effect (EC_{50}) values of 50% towards *F. graminearum* and *C. mebaldsii* were further measured (Figure 5 and Table 5). This demonstrated that compounds **1** and **2** possessed 15.7 and 42.1 mg/L EC_{50} values against *C. mebaldsii*, *respectively*, while the fungicidal levels were superior to that of hymexazol (84.8 mg/L). In addition, the EC_{50} values of compounds **1** (68.8 mg/L) and **2** (78.0 mg/L) against *F. graminearum* were close to that of hymexazol (66.3 mg/L). This finding suggested that compounds **1** and **2** could be potential alternative lead compounds for the design of fungicides.

Table 4. Fungicidal activities of compounds **1**–**7** at 80 mg/L.

Cpd.	FG *	CM	CL	BC	AA	SS	RS
1	61.4 ± 4.3	80.0 ± 5.3	54.5 ± 0.0	36.2 ± 7.9	53.3 ± 2.9	61.4 ± 6.1	56.0 ± 9.2
2	55.7 ± 6.5	60.0 ± 2.7	51.5 ± 2.6	55.2 ± 6.0	53.3 ± 2.9	36.8 ± 13.9	52.0 ± 0.0
3	65.7 ± 0.0	NT **	47.0 ± 2.6	56.9 ± 6.0	51.7 ± 2.9	66.7 ± 8.0	38.0 ± 3.5
4	58.6 ± 2.5	NT	NT	34.5 ± 7.9	51.7 ± 5.8	49.1 ± 13.2	40.0 ± 0.0
5	54.3 ± 6.5	72.3 ± 0.0	NT	56.9 ± 3.0	63.3 ± 2.9	40.4 ± 8.0	40.0 ± 6.0
6	37.1 ± 4.9	NT	NT	5.2 ± 3.0	13.3 ± 2.9	36.8 ± 0.0	20.0 ± 3.5
7	NT	NT	NT	34.5 ± 6.0	NT	33.3 ± 3.0	NT
hymexazol	61.4 ± 0.0	50.8 ± 2.7	83.3 ± 2.6	70.7 ± 3.0	66.7 ± 2.9	61.4 ± 3.0	62.0 ± 3.5

* FG: Fusarium graminearum; CM: Curvularia mebaldsii; CL: Curvularia lunata; BC: Botrytis cinerea; AA: Alternaria altanata; SS: Sclerotinia sclerotiorum; RS: Rhizoctonia solani. ** NT means no test.

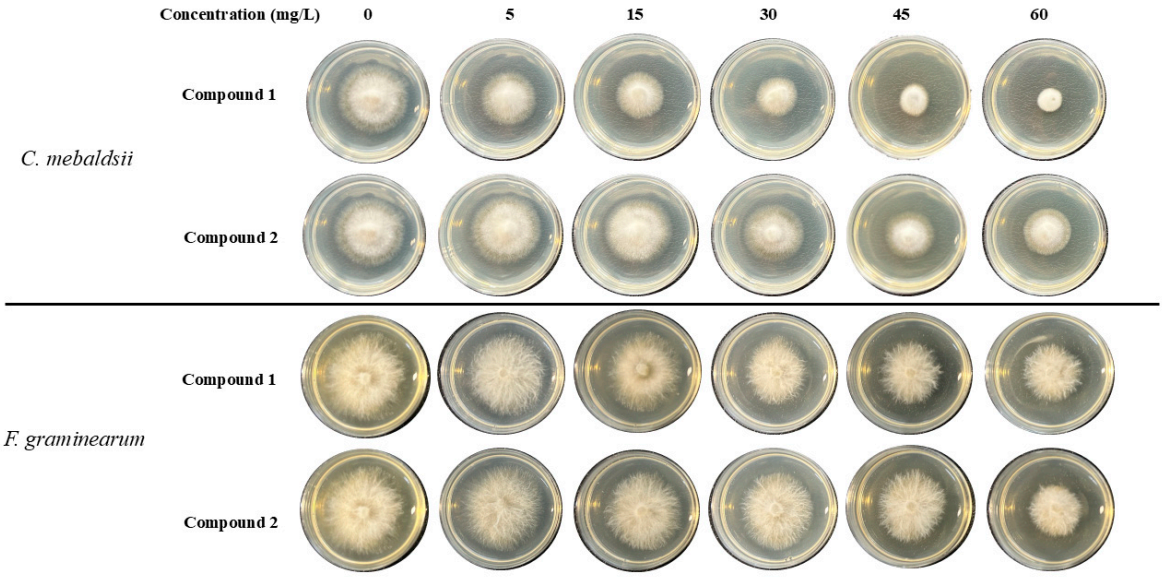

Figure 5. The fungicidal efficacy of compounds **1** and **2**.

Table 5. The EC_{50} values of compounds **1** and **2**.

	Compound	R2	Regression Equation (y = ax + b)	EC_{50} (mg/L)
C. mebaldsii	**1**	0.943	y = 1.171x + 3.601	15.7
	2	0.950	y = 0.712x + 3.844	42.1
	hymexazol	0.953	y = 2.314x + 0.537	84.8
F. graminearum	**1**	0.961	y = 1.426x + 2.381	68.6
	2	0.983	y = 1.369x + 2.410	78.0
	hymexazol	0.961	y = 1.561x + 2.157	66.3

3. Experimental Section

3.1. Fungal Material

The origin and verification of *P. euphratica* resins matched our previous study [6], and the voucher specimen (CHYX0573) was stored at Shenzhen University.

3.2. Extraction and Isolation

The dried resins (50.0 kg) were soaked in 95% ethanol (300 L × 3 × 24 h) to produce a crude extract, which was then mixed with water and separated using ethyl acetate. Subsequently, the EtOAc solution was concentrated under reduced pressure to produce a 12.0 kg EtOAc soluble extract. Subsequently, the extract underwent separation by multiple chromatography, obtaining compounds **1**–**7**. For additional detailed isolation procedures, consult the Supplementary Information.

3.3. Crystal Structure of **1**

The crystallographic information for euphraticanoid N (**1**) (deposition number CCDC 2422553) is available at the Cambridge Crystallographic Data Centre. You can access the data for free at www.ccdc.cam.ac.uk/data_request/cif (accessed on 15 February 2025), or by emailing data request@ccdc.cam.ac.uk, or by contacting The Cambridge Crystallographic Data Centre, 12 Union Road, Cambridge CB2 1EZ, UK; fax: +44 1223 336033.

3.4. ECD Calculations for Compounds **1**–**7**

The main conformers of compounds **1**–**7** were optimized using Gaussian 09 at the B3LYP/6-311g(d,p) level. Then, we used the same method for the optimized conformers

for the ECD calculations. Solvent effects were incorporated using the PCM model, with methanol serving as the solvent. The percentages of each conformation can be found in Table S3. The ECD spectra were ultimately derived from the Boltzmann-calculated contribution of each conformer.

3.5. Fungicidal Activity Assay

The fungicidal activity of compounds **1**–**7** was evaluated against the fungal strains using the method according to the literature [11–14]. Briefly, pathogen mycelial plugs (diameter 0.4 cm) were adhered to the center of potato dextrose agar (PDA) plates containing specific concentrations of the compounds (with equal volumes of DMSO as a control). The plates were cultivated at 26 °C for three days, and the colony diameter was measured in triplicate to assess the growth rate. The inhibition rates were identified using the formula $I\% = [(C - T)/(C - 0.4)] \times 100\%$. Here, C means the diameter of fungal growth treated by DMSO; T means the diameter of fungal growth treated by the compounds; and I means the inhibition rate. An average was taken, and the standard deviation was measured.

4. Conclusions

To conclude, the current study led to the identification of five prenylaromadendrane-type diterpenes (**1**–**5**) and two aromadendrane-type sesquiterpenes (**6** and **7**) from *P. euphratica* resins. In addition, the fungicidal activities of compounds **1**–**7** were evaluated. The bioassay results revealed that compound **1** displays potent fungicidal activities against *C. mebaldsii* and *F. graminearum* with the EC_{50} values of 15.7 and 68.6 mg/L, respectively. According to our knowledge, this is one of few studies on fungicidal agents derived from *P. euphratica*, providing an innovative structural model for fungicide design.

Supplementary Materials: The following supporting information can be downloaded at https://www.mdpi.com/article/10.3390/ijms26052187/s1: NMR data for ^{1}H and ^{13}C in $CDCl_3$ of **2**–**4**, along with general procedures, detailed isolation procedures, characterization data, and NMR, HRESIMS, UV, and CD spectra for compounds **1**–**7**, as well as X-ray crystallography data for compound **1**. ECD calculations for compounds **1**–**7** can also be found here. Reference [15] are cited in the Supplementary Materials.

Author Contributions: Y.-X.C. was responsible for the conception and design of the experiments and the paper, while Q.J. and D.H. conducted the biological experiments. Y.-Y.L. executed the chemical experiments. D.H. reviewed and revised the paper. All authors have read and agreed to the published version of the manuscript.

Funding: This research received financial support from the Shenzhen Fundamental Research Program (JCYJ20200109114003921).

Institutional Review Board Statement: Not applicable.

Informed Consent Statement: Not applicable.

Data Availability Statement: All the data in this research are presented in manuscript and Supplementary Materials.

Conflicts of Interest: The authors declare no conflicts of interest.

References

1. Chaudhary, G.; Ewoldt, R.H.; Thiffeault, J.L. Unravelling hagfish slime. *J. R. Soc. Interface* **2019**, *16*, 20180710. [CrossRef]
2. Macleod, R.; Sinding, M.S.; Olsen, M.T.; Collins, M.J.; Rowland, S.J. DNA preserved in jetsam whale ambergris. *Biol. Lett.* **2020**, *16*, 20190819. [CrossRef] [PubMed]

3. Frank, E.T.; Kesner, L.; Liberti, J.; Helleu, Q.; LeBoeuf, A.C.; Dascalu, A.; Sponsler, D.B.; Azuma, F.; Economo, E.P.; Waridel, P.; et al. Targeted treatment of injured nestmates with antimicrobial compounds in an ant society. *Nat. Commun.* **2023**, *14*, 8446. [CrossRef] [PubMed]
4. Liu, C.; Zhou, G.; Liu, J. Isolation and screening of fungi for enhanced agarwood formation in *Aquilaria sinensis* trees. *PLoS ONE* **2024**, *19*, e0304946. [CrossRef] [PubMed]
5. Ching, Y.H.; Lin, F.M.; Chen, H.C.; Hsu, C.Y.; P'ng, S.Y.; Lin, T.N.; Wang, Y.C.; Lin, C.J.; Chen, Y.C.; Ho, T.J.; et al. Hypoglycemic effects of dracorhodin and dragon blood crude extract from *Daemonorops draco*. *Bot. Stud.* **2024**, *65*, 8. [CrossRef] [PubMed]
6. Dang, W.; Guo, T.; Zhou, D.; Meng, Q.; Fang, M.; Chen, G.; Lin, B.; Hou, Y.; Li, N. Structure-guided isolation of anti-neuroinflammatory sesquiterpene coumarins from *Ferula sinkiangensis*. *Chin. J. Nat. Med.* **2024**, *22*, 643–653. [CrossRef] [PubMed]
7. Sura, M.B.; Cheng, Y.X. Medicinal plant resin natural products: Structural diversity and biological activities. *Nat. Prod. Rep.* **2024**, *41*, 1471–1542. [CrossRef] [PubMed]
8. Liu, Y.Y.; Huang, D.L.; Dong, Y.; Qin, D.P.; Yan, Y.M.; Cheng, Y.X. Neuroprotective norsesquiterpenoids and triterpenoids from *Populus euphratica* resins. *Molecules* **2019**, *24*, 4379. [CrossRef] [PubMed]
9. Anjaneyulu, A.S.R.; Krishnamurthy, M.V.R.; Rao, G.V. Rare Aromadendrane diterpenoids from a new soft coral speciesof *Sinularia Genus* of the indian ccean. *Tetrahedron* **1997**, *53*, 9301–9312. [CrossRef]
10. Wang, Y.G.; Ren, J.; Wang, A.G.; Yang, J.B.; Ji, T.F.; Ma, Q.G.; Tian, J.; Su, Y.L. Hepatoprotective prenylaromadendrane-type diterpenes from the gum resin of *Boswellia carterii*. *J. Nat. Prod.* **2013**, *76*, 2074–2079. [CrossRef] [PubMed]
11. Xie, J.; Xu, W.; Song, H.; Liu, Y.; Zhang, J.; Wang, Q. Synthesis and antiviral/fungicidal/insecticidal activities study of novel chiral indole diketopiperazine derivatives containing acylhydrazone moiety. *J. Agric. Food Chem.* **2020**, *68*, 5555–5571. [CrossRef] [PubMed]
12. Liao, A.; Li, L.; Wang, T.; Lu, A.; Wang, Z.; Wang, Q. Discovery of phytoalexin camalexin and its derivatives as novel antiviral and antiphytopathogenic-fungus agents. *J. Agric. Food Chem.* **2022**, *70*, 2554–2563. [CrossRef] [PubMed]
13. He, H.W.; Xu, D.; Wu, K.H.; Lu, Z.Y.; Liu, X.; Xu, G. Discovery of novel salicylaldehyde derivatives incorporating an α-methylene-γ-butyrolactone moiety as fungicidal agents. *Pest Manag. Sci.* **2023**, *79*, 5015–5028. [CrossRef] [PubMed]
14. Wang, J.; Liu, H.; Jiang, J.; Liu, X.; Zhou, T.; Li, J.Q.; Xiao, Y.; Qin, Z. Discovery of triphenylphosphonium (TPP)-conjugated N-(1,1′-biphenyl)-2-yl aliphatic amides as excellent fungicidal candidates. *Pest Manag. Sci.* **2023**, *79*, 2920–2933. [CrossRef] [PubMed]
15. Frisch, M.J.; Trucks, G.W.; Schlegel, H.B.; Scuseria, G.E.; Robb, M.A.; Cheeseman, J.R.; Scalmani, G.; Barone, V.; Mennucci, B.; Petersson, G.A.; et al. *Gaussian 09, Revision D.01*; Gaussian, Inc.: Wallingford, CT, USA, 2009.